Still a Threat: Polychlorinated Biphenyl (PCB) Metabolism in Cells & Formation of Cancer-Causing DNA Adducts

Keywords: DNA Adducts, PCBs, Polychlorinated Biphenyls, Mass Transfer, COMSOL

BEE 4530: Computer-Aided Engineering | Applications to Biological Processes

Table of Contents

1. Executive Summary

Despite PCBs having been banned from manufacturing processes for decades, polychlorinated biphenyls or PCBs can still enter the environment through various means, such as improper waste disposal methods, and wreak havoc. Current PCB-containing products are those that predate the ban but persistent health risks still exist due to the PCB chemical stability in the environment. Exposure to PCBs through inhalation, ingestion, increase risk of developing multiple medical problems, particularly cancer. Once PCBs diffuse into a cell, metabolites are produced by a cascade of reactions. PCB metabolites can then bind to DNA to create DNA adducts. This process results in mutations that can gradually develop into cancer.

We hope to gain a better understanding of the impact of PCB exposure by modeling cellular PCB metabolism and DNA adduct formation with COMSOL Multiphysics 5.5. Mass transfer modules (including reaction, partitioning, and diffusion) were used to model PCB and PCB metabolite movement and accumulation in a cell over time. We modelled one spherical cell with 1D axisymmetric geometry divided into five distinct domains. Factors including temperature, pH level, and organelle interactions (besides the nucleus) were disregarded. We also assumed a uniform enzyme concentration of 0.25 μM for all enzymatic reactions. Key parameters including diffusion coefficients, some rate constants, and partitioning coefficients were referenced from similar work by Chaudhry et al. and the SABIO-RK database.

Damage to the cell was quantified via the number of DNA adducts formed. Model validation was done by comparing the DNA adducts concentration of our COMSOL model, with published literature values. The final number of DNA adducts calculated by our COMSOL model was 10^4 times greater than the DNA adducts values from literature. The sensitivity analysis found the DNA adduct formation rate constant to be the most sensitive rate constant impacting the final DNA adduct concentration. It is possible that an incorrect DNA adduct formation rate could result in deviation from experimental results. It is also possible for incorrect rate constants to have a comparatively smaller effect on final DNA adduct values.

Accurate quantification of DNA adducts formed from a specified PCB exposure time and concentration may allow quantification of a cancer risk from DNA adduct formation. If a specified level of acceptable DNA adduct formation and cancer risk was selected, maximum allowable exposure time and concentration will be known. Maximum allowable concentration can act as a design constraint for water treatment, soil remediation, and other treatment efforts. Accurate quantification of DNA adduct formation may further replace or supplement *in vitro* experimentation requiring ^{32}P-post labeling or high performance liquid chromatography (HPLC), as well as *in vivo* experimentation, saving resources involved with live cell experiments.

Keywords: DNA Adducts, PCBs, Polychlorinated Biphenyls, Mass Transfer, COMSOL

2. Introduction

Polychlorinated biphenyls (PCBs) were widely used in manufacturing processes prior to their ban in the 1970s [1]. PCBs are highly chemically stable and non-flammable due to their inertness [2]. These properties made PCBs highly desirable for use in a wide range of products, including transformers and capacitors, hydraulic fluids, paint, and carbonless paper [1], [2]. This resistance to thermal and chemical degradation allows PCBs to persist in the environment [3]. Mismanagement and improper disposal methods release PCBs into the air, soil, and water, where they leach into the surrounding soil and water [3]. PCBs can then enter the human body through inhalation or ingestion [3]. Increased exposure to PCBs, through prolonged or repeated exposure, can damage human health over time [3].

Although PCBs are not utilized in current manufacturing processes, exposure is still possible through the demolition, dysfunction, or uncontrolled recycling of PCB-containing structures and equipment [4]. The most common mode of exposure for humans is consumption of PCB-contaminated food [4]. The lipophilic nature of PCBs, which allows them to accumulate in lipids or fats, leads to bioaccumulation in organisms like fish and bivalves [2]. Consumption of contaminated organisms exposes humans to relatively high amounts of PCBs [2]. For example, PCBs that entered a body of water through accidental or purposeful dumping can accumulate in the fatty tissue of the fish residing in the water body. These contaminated fish can transfer PCBs to any creature that consumes it, including humans.

PCB exposure is associated with hepatotoxicity, neurotoxicity, immunotoxicity, hormone disruption, and carcinogenicity [2]. PCBs induce formation of reactive oxygen species and have genotoxic effects [4]. At the cellular level, certain PCB-metabolites produced by the activity of cellular enzymes can bind to DNA strands, forming DNA adducts [2]. These DNA adducts may be carcinogenic [2]. This link between PCB exposure and carcinogenesis led the EPA to ban PCB use in 1979 [3]. Although this policy forbids the use of PCBs in modern manufacturing practices, PCBs in products predating this ban still pose significant environmental and health risks. In 2011, regions in Chicago, Italy, and Germany experienced air exposure to PCBs [5]. Despite regulations limiting allowable levels of PCBs for schools in Germany, some regions still exceeded these levels [5]. Regulatory monitoring of PCB levels in water, fish, and sediment in the Great Lakes and other regions of the USA failed to recognize airborne PCBs [5]. Hu et al. discovered diarylide yellow, a PCB-containing pigment, in the ambient air of Chicago, Illinois [6]. In 2009, Rodenburg et al. showed that this pigment, in consumer goods such as newspapers, magazines, food packaging, and plastic bags in regions where wastewater treatment plants release waste [7]. There was also evidence of PCB within the New York/New Jersey Harbor and the Delaware River and occurring in even greater concentrations downstream [7].

Current toxicology studies rely on live cell cultures to observe the negative effects of exposure to organic pollutants. DNA adduct formation from PCB-metabolites has been examined in multiple studies [2], [11], [3]. However, these studies typically do not use whole cells [2], [11], [3]. Typically, PCBs are mixed with enzymes, which convert them to their metabolites. These metabolites then form adducts with the provided DNA sample [3], [11]. In other studies, a PCB metabolite may be chemically formed and directly inoculated with DNA [2]. These studies provide a basis for quantifying DNA adducts formation, but do

not include dynamics of the entire cell.

Digitally modeling the entry and intracellular travel of PCBs will improve understanding of their toxicological effects on human cells while avoiding the time, cost, and ethical issues of live cell work [8]. To address this need, we developed and executed a model on COMSOL to quantify the changes in the concentrations of PCB and reactive PCB metabolites over time. We designed our model to expand upon available knowledge on lipophilic compound metabolism and fate in cells, and, by extension, the carcinogenic risk of these compounds. Previously, Chaudhry et al. performed a COMSOL simulation of the diffusion of lipophilic compounds and their reactions in the extracellular matrix and cell, including DNA adduct formation [9]. However, their model was focused on polycyclic aromatic hydrocarbons (PAHs) [9]. Both PAHs and PCBs are lipophilic and can produce metabolites that form DNA adducts. However, PCBs undergo different reactions at different speeds and form different products [10]. The PCB model discussed in this paper includes different reactions versus Chaudhry et al.'s PAH model and uses dilute species mass transport instead of reaction engineering in COMSOL Multiphysics 5.5 [9].

The COMSOL model presented in this paper references several components from the model developed by Chaudhry et al., including the processes involved (diffusion, reaction, and partitioning), the geometry and boundary conditions, and the diffusion and partition coefficients [9]. However, we focused on quantifying carcinogenic DNA adduct formation from PCB metabolites, as opposed to PAH. In both models, the penetration and eventual accumulation of carcinogenic organic pollutants in mammalian cells were depicted as a series of mass transfer processes — specifically, reaction and diffusion - taking place across five domains: the extracellular matrix (EC), the cell membrane, the cytoplasm, the nuclear membrane, and the nucleus. The designs of both models also factored included membrane absorption and desorption and reactions resulting in reactive metabolites, as well as other factors with the potential to affect pollutant diffusion, such as a simplified cell geometry. We also quantified the concentration of (semi)quinones, since they contribute to DNA adduct formation [12]. The accuracy of the model was assessed using data obtained from previous experiments in this subject.

2.1 Problem Statement

DNA adducts can impede DNA replication and repair, which can lead to the development of carcinogenic mutations [10]. Cellular uptake of PCBs and subsequent accumulation of PCB metabolites within the cell results in DNA adduct formation within the nucleus, specifically via bonding of quinones or arene oxides to DNA [14]. PCB diffuses from the extracellular matrix through the cell membrane into the cytoplasm [9]. In the cytoplasm, the cell metabolizes PCB into arene oxides and PCB-OHs [16]. Arene oxides then form diols and glutathione conjugates [14]. The diols are eventually transformed to quinones. Both quinones and arene oxides then diffuse into the nucleus through the nuclear membrane and bind to DNA to form DNA adducts [14].

No COMSOL models of PCB metabolism and subsequent DNA adduct formation within a cell currently exist as far as we know. This model was created using experimental data of enzyme kinetics, PCB degradation intermediates and products, and DNA adduct formation data. Specific model geometry design

was referenced from Chaudhry et al. [9]. Further design applications of our model are described in Section 5.

2.2 Design Objectives

The main objectives of this study are:

1. To understand cellular metabolism of persistent organic pollutants (PCB).
2. To model the transport, transformation, and accumulation of PCB metabolites, particularly those capable of forming DNA adducts, in the cell.
3. To quantify DNA adduct formation from PCB-metabolites as a result of PCB exposure.

By designing a model that addresses these questions, we aimed to gain a more thorough understanding of a phenomenon that is mostly understood and discussed at a macroscopic level with whole body animal models. Whole-body toxicology studies typically quantify lethality resulting from acute exposure to PCB but do not explore how toxicity and damage accumulates over a period of time in individual cells. Our goal in developing this model was to observe and quantify the effects of PCB accumulation on DNA adduct formation within human cells.

3. Methods

3.1 Schematic

Consumption of PCB-contaminated fish is one of many possible methods of PCB exposure for humans (Fig. 1) [2]. PCBs diffuse from the extracellular environment through the membrane and into the cytoplasm [14]. PCB is metabolized into various metabolites by enzymes and other processes [14]. Quinones and arene oxides form and diffuse through the nuclear membrane and into the nucleus, where they can bind to and damage DNA through adduct formation [14].

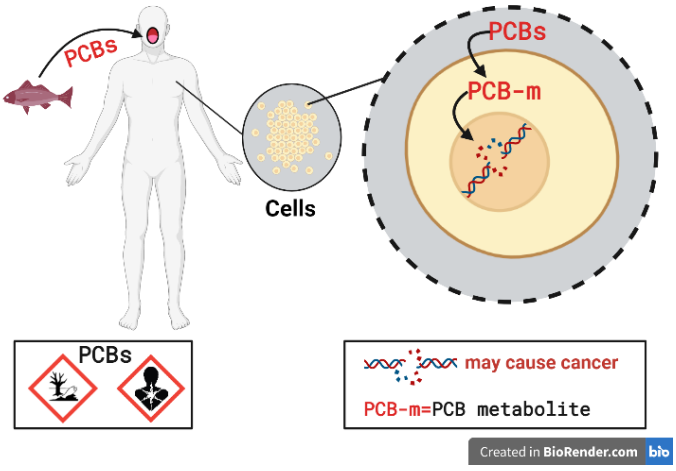

Fig. 1 Simplified pathway of human DNA-adduct formation from PCB exposure via fish consumption

3.2 Model Geometry and Setup

Our current model will focus on how PCB and PCB metabolites within a cell. Important cell model geometry is listed in Table 1. The following assumptions have been made for our model setup:

1. Cell geometry was assumed to be spherical and uniform.
2. Cell membrane and nuclear membrane were assumed to be uniform thickness.
3. Enzyme concentration was 0.25 um for all enzymes.
4. Uniform diffusion coefficient values were used for all chemical species within each domain.
5. Reactions and diffusion were independent of temperature and pH.
6. The cell contained no organelles.
7. The cell exists as a single cell.

Table 1: Important Cell Geometry Values.

Important Model Geometry	Value	Unit
CHO Cell Diameter [15]	14	um
Nucleus Diameter [16]	3	um
Cell Volume [15]	179	um^3
Nucleus Volume (8% total cell volume) [16]	14.32	um^3
Cell Membrane Thickness [17]	10	nm
Nucleic Membrane Thickness [11]	10	nm

Based on these assumptions, we simplified the 3D diffusion and reaction to a 1D axisymmetric geometry, as shown in Fig. 2A and 2B below. Table 2 lists the reactions and diffusion processes occurring in each domain.

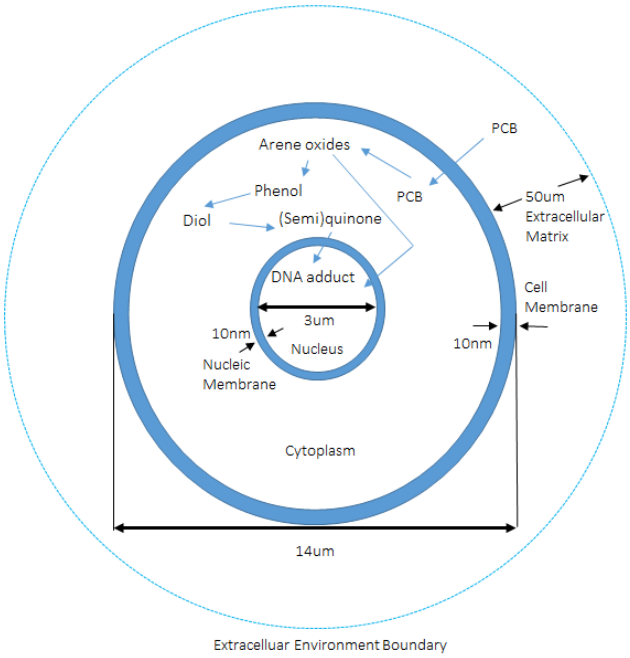

(A)

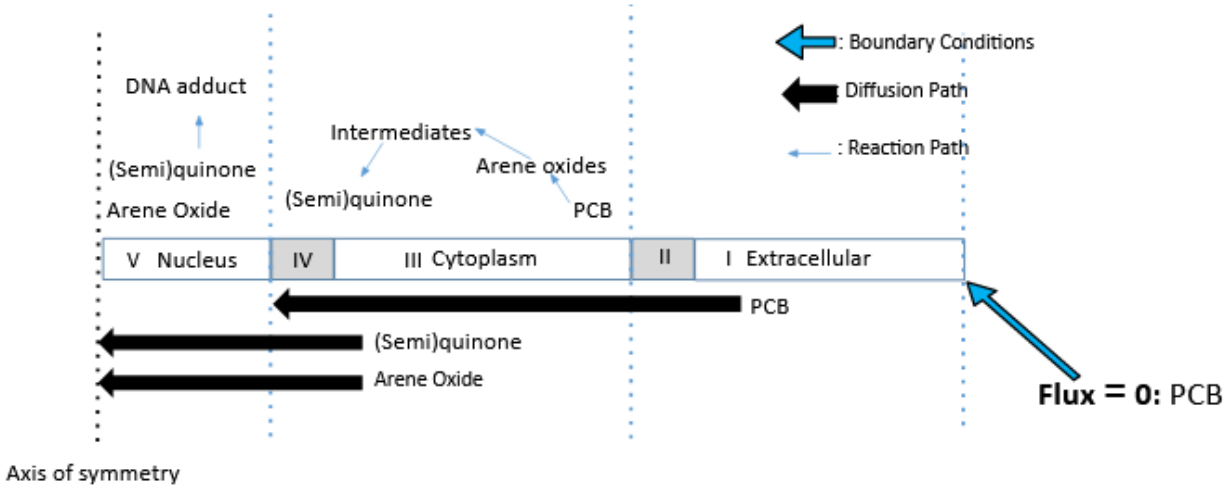

(B)

Fig. 2 PCB diffusion and reaction schematic. (A) indicates the 2D cell diagram. (B) indicates a cross section of the 2D cell in (A).

Table 2: Reaction and Diffusion for Each Species and Domain

Domain	Diffusion Species	Diffusion Path	Reaction
I	PCB	I-->II	/
II	PCB	II-->III	/
III	PCB	III-->IV	PCB -->Arene oxide [14]
	Arene oxide	Limited within III [9]	Arene oxide-->Diol [14]
	Diol		Diol-->Diol2 [14]
	Diol2		Dio2l-->(Semi)quinone [14]
	(Semi)quinone	III-->IV	/
IV	PCB	IV-->V	/
	(Semi)quinone		
V	PCB	Limited within V [9]	/
	(Semi)quinone		(Semi)quinone+DNA-->DNA adduct [14]

3.3 Governing Equations and Boundary Conditions

3.3.1 General Governing Equation (spherically symmetrical)

Equation 1 shows the general form of the mass transfer equation for spherically symmetric coordinates The equation includes generation and depletion from reactions and partitioning, This was used in all domains to account for the diffusion process.

$$\frac{\partial c_i}{\partial t} = D_{i,j}\frac{1}{r^2}\frac{\partial}{\partial r}\left(r^2\frac{\partial c_i}{\partial r}\right) + r_i \quad (1)$$

c_i is the concentration of species $i$where i = Q, PCB, or another species, $D_j$is the diffusivity of domain j where species i is located, and r_i is the reaction term of species i. As shown in the Fig. 2B, the cell model has 5 domains. Table 3 shows the transport species and the reactions in each of the domains, where k_i is the rate constant for a species. Appendix A Table 12 lists the values of the parameters for these equations.

3.3.2 Boundary Conditions

The outer boundary of the extracellular matrix is assumed to experience no species flux to create a closed system.

$$\frac{\partial C_i}{\partial r}|_{r=57,\ t} = 0 \tag{2}$$

Species A (DNA adducts) is restricted to the nucleus (V).

$$\frac{\partial Add}{\partial r}|_{1.5=r,\ t} = 0 \tag{3}$$

Species GC (glutathione conjugates), PCB-OH (PCB hydroxide) and L/L2 (diols) are restricted to the cytoplasm (III). PCBs also do not enter the nucleus or nuclear membrane.

$$\frac{\partial AO-GC}{\partial r}|_{r\,=\,1.51,r\,=6.99\ \ t} = 0 \tag{4}$$

$$\frac{\partial PCB-OH}{\partial r}|_{r\,=\,1.51,r\,=6.99\ \ t} = 0 \tag{5}$$

$$\frac{\partial L}{\partial r}|_{r\,=\,1.51,r\,=6.99\ \ t} = 0 \tag{6}$$

$$\frac{\partial L2}{\partial r}|_{r\,=\,1.51,r\,=6.99\ \ t} = 0 \tag{7}$$

$$\frac{\partial PCB}{\partial r}|_{r\,=\,1.51\ \ t} = 0 \tag{8}$$

PCBs diffuse into the cell from the extracellular matrix

$$\frac{\partial PCB}{\partial r}|_{r\,=\,7,\ t} \ncong 0 \tag{9}$$

Partition coefficients impact the concentrations in all 5 domains. At the boundary between membranes and aqueous domains (cytoplasm, EC matrix, nucleus), the partition coefficient partitions the species based on the following equations.

$$k_p = \frac{C_{aqueous}}{C_{lipid}} \tag{10}$$

For PCB;

$$k_p = \frac{C_{EC\,matrix}}{C_{membrane}}|_{r=7,t} \tag{11}$$

$$k_p = \frac{C_{cytoplasm}}{C_{membrane}}|_{r=6.99,t} \tag{12}$$

For quinone(Q) and arene oxide (AO);

$$k_p = \frac{C_{cytoplasm}}{C_{nuc.membrane}}|_{r=1.51,t} \tag{13}$$

$$k_p = \frac{C_{nucleus}}{C_{nuc.membrane}}|_{r=1.5,t} \tag{14}$$

3.3.3 Initial Conditions

At time 0, before reactions start, PCB is the only species. Species names are listed in Table 3.

$$AO = 0|_{r,\ t=0} \tag{15}$$

$$L = 0|_{r,\ t=0} \tag{16}$$

$$L2 = 0|_{r,\ t=0} \tag{17}$$

$$PCB - OH = 0|_{r,\ t=0} \tag{18}$$

$$Q = 0|_{r,\ t=0} \tag{19}$$

$$A = 0|_{r,\ t=0} \tag{20}$$

$$AO - GC = 0|_{r,\ t=0} \tag{21}$$

At time 0, PCBs are only in the extracellular matrix.

$$PCB = 0|_{r<7,\ t=0} \tag{22}$$

Table 3: Transport Species and Reactions of Corresponding Species

Domain	Transport Species	Diffusion	Reaction ($\frac{\partial c_i}{\partial t}$)
Extracellular Matrix(1)	PCB	Occurs	
Cell Membrane (2)	PCB	Occurs	Partitioning: $k_P = C_{water}/C_{lipid}$ [9]
Cytoplasm (3)	PCB3	Occurs	$-(k_{AO}c_{PCB}) - (k_{PCB-OH}c_{PCB})$
	Arene Oxides (AO)	Occurs	$(k_{AO}c_{PCB}) - (k_{AO-GC}c_{AO} + k_L c_{AO})$
	PCB-OH		$(k_{PCB-OH}c_{PCB})$
	Diols (L)		$(k_L c_{AO}) - (k_{L2}c_L)$
	Diols w. Cl (L2)		$(k_{L2}c_L) - (k_Q c_{L2})$
	Quinones (Q)	Occurs	$k_Q \times \frac{(k_{L2}[(k_{L\times}c_{AO})/(1+k_{L2})])}{1+k_Q}$
	Glutathione Conjugates (AO-GC)		$(k_{AO-GC}c_{AO})$
Nuclear Membrane (4)	Quinones	Occurs	Partitioning: $k_P = C_{water}/C_{lipid}$ [9]
	Arene Oxides	Occurs	
Nucleus (5)	Arene Oxides	Occurs	$-(k_{Add}c_{AO})$
	Quinones	Occurs	$-(k_{Add}c_Q)$
	DNA Adducts (A)		$(k_{Add}c_Q + k_{Add}c_{AO})$

4. Results

Parameters used are listed in Appendix A Table 12. Intermediates like AO-GC, L, L2, and PCB-OH were incorporated in reactions only, as opposed to having their own diffusion physics. Time period considered was 3600 seconds.

Fig. 3A-E below shows the PCB concentration at early time points. PCB quickly diffuses into the cytoplasm, as expected. The EC matrix concentration decreases as more PCB is pulled into the cytoplasm.

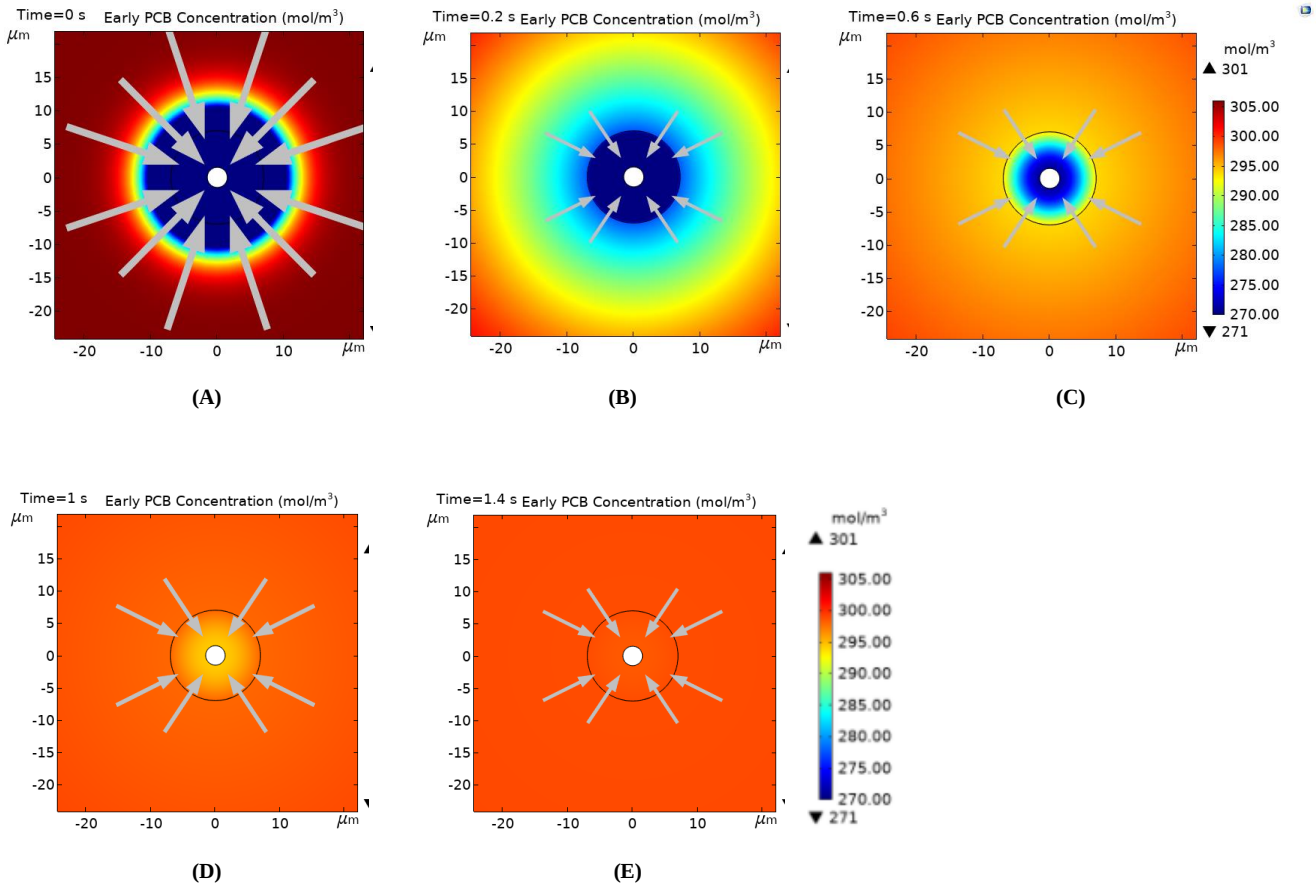

Fig. 3 Concentration of PCB at early time points: ((A) = 0 s, (B) = 0.2 s, (C) = 0.6 s, (D) = 1 s, (E) = 1.4 s)

As Fig. 4 shows, cytoplasm PCB concentration is reduced as it forms PCB-OH and AO. When the cytoplasm PCB concentration decreases, more PCB diffuses in from the EC matrix due to the lowered cytoplasm concentration.

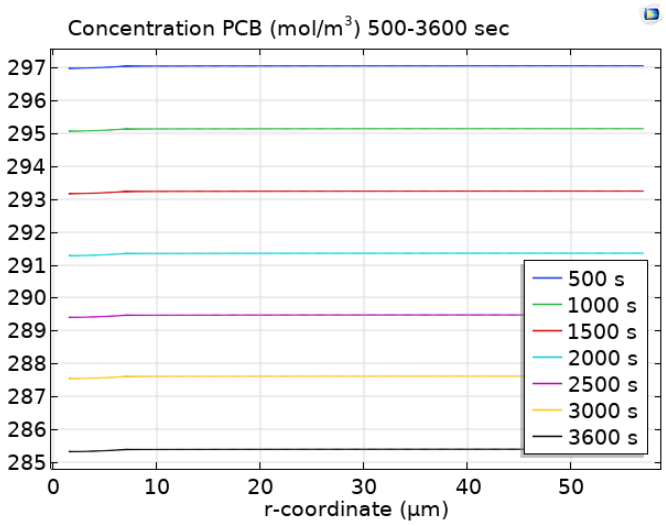

Fig. 4: PCB concentration from 500 to 3600 s

The concentration at the final time point, 3600 s, is about 285.5 mol/m^3. It is likely that running this solution for more time will continue to decrease the EC and cytoplasm PCB concentration. Fig. 3A-E and Fig. 4 together show that PCB concentration between the cytoplasm and nucleus becomes relatively uniform within the first few seconds, meaning there is little difference between the cytoplasm and EC concentrations. The balancing and reduction of PCB concentration is as predicted for this model based on the principles of diffusion.

The membrane concentration of PCB is shown in Fig. 5. Due to PCB's lipophilic nature, the membrane concentration is much higher than the surrounding concentration.

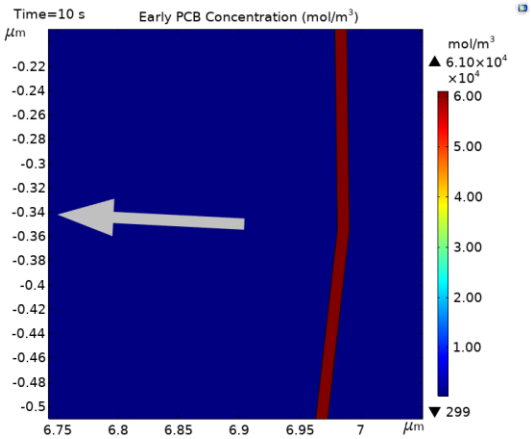

Fig. 5: PCB concentration in cell membrane at 10 sec

Fig. 6A below shows the arene oxide (AO) concentration at early time points in the nucleus and cytoplasm. After it forms from PCB, AO quickly diffuses from the cytoplasm into the nucleus.

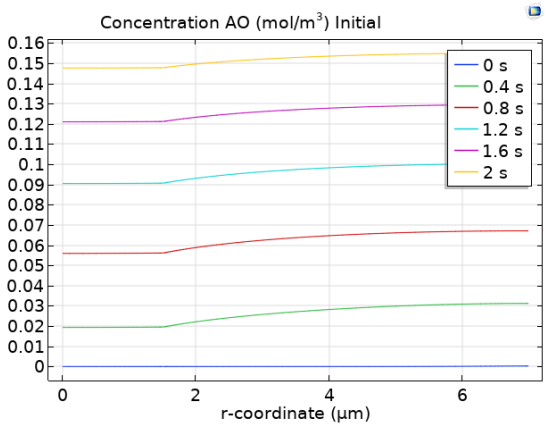

(A)

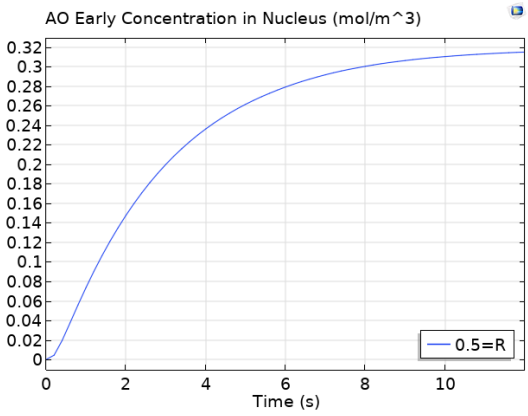

(B)

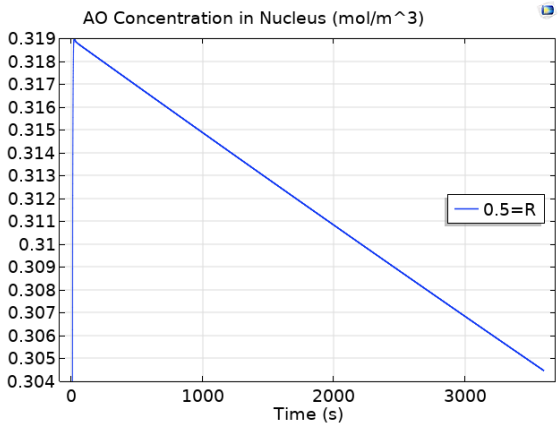

(C)

Fig. 6: AO concentration at early time points in the cytoplasm & nucleus (A), AO concentration for the first 12 s at R=0.5 (B) and AO concentration over time at R=0.5 (C)

There is little difference (~0.01 mol/m^3) between the nucleus and cytoplasm concentrations in Fig. 6A, which is likely due to the small size of the nucleus. The shorter the distance between different concentrations, the more quickly diffusion occurs. Fig. 6B and Fig. 6C show that arene oxide quickly reaches a maximum concentration (within the first 12 seconds) before being depleted by formation of glutathione conjugates (AO-GC), diols (which lead to quinones), and DNA adducts.

Fig. 6B shows how quickly AO concentration in the nucleus reaches its maximum. Fig. 6C shows the subsequent depletion of AO in the nucleus. AO concentration in the cytoplasm is depleted by conversion to AO-GC, diols, and diffusion into the nucleus. AO concentration in the nucleus is depleted by conversion to adducts.

The same species and time period was examined in the cytoplasm. The trend and concentration values are the same.

Fig. 7A below shows the quinone (Q) concentration at early time points. Its concentration seems to increase quickly due to the fact that the concentration is very small, so small differences seem more significant.

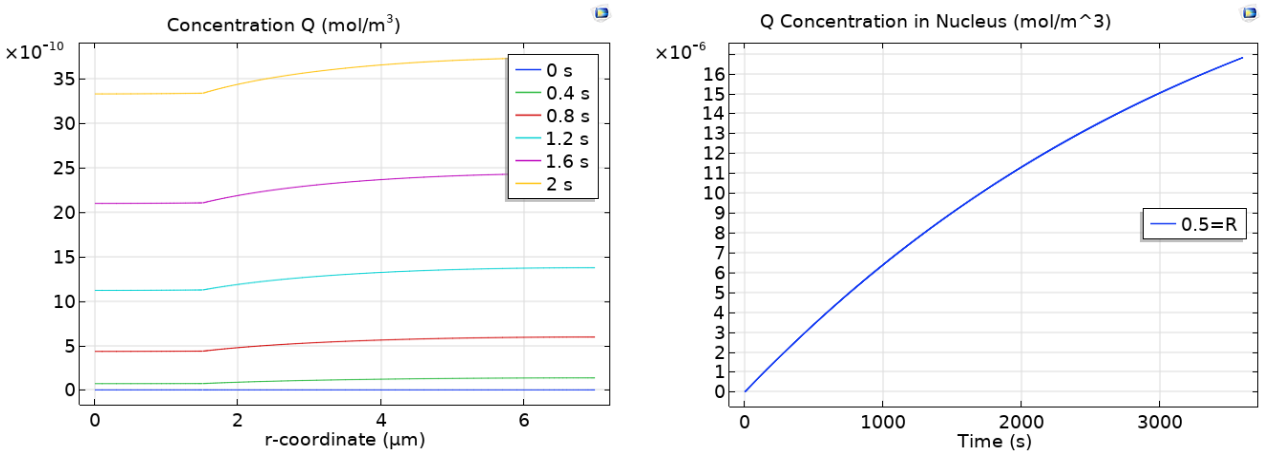

(A) **(B)**

Fig. 7: Initial Q concentration in the cytoplasm & nucleus (A) and Q concentration over time at R=0.5 um

Fig. 7A includes concentrations on the order of 10^{-10} mol/m^3. This very small early concentration is due to the relatively small rate of formation of Q. In particular, the formation rate of L2 from L is very small (AO → L → L2 → Q).

Fig. 7B shows Q concentration increasing over the entire 3600 second study.

Q concentration is on the order of 10^{-4} mol/m^3 from 500 to 3600 seconds, or most of the study. Q concentration is still very small due to the small rate of formation. There is also very little, if any, difference between the nucleus and cytoplasm concentration shown in Fig. 7A. As with AO, this is likely due to the fast rate of diffusion associated with small distances.

Fig. 6C and Fig. 7B show the opposing trends of AO and Q concentrations over the same location and time. Unlike AO, Q concentration increases continuously and may continue increasing beyond 3600 seconds. This is likely due to the fact that AO is depleted by three reactions, while Q is depleted by one reaction. Despite the difference in trends, the Q concentration is 10^{-3} smaller than the AO concentration during the course of this study.

As with PCB, the concentration of Q and AO in the nuclear membrane is much higher than the surrounding aqueous concentration. This is expected based on the partition coefficient.

Fig. 8 below shows the DNA adduct concentration over time in the nucleus. It forms from two species, is not degraded, and has a relatively high rate constant.

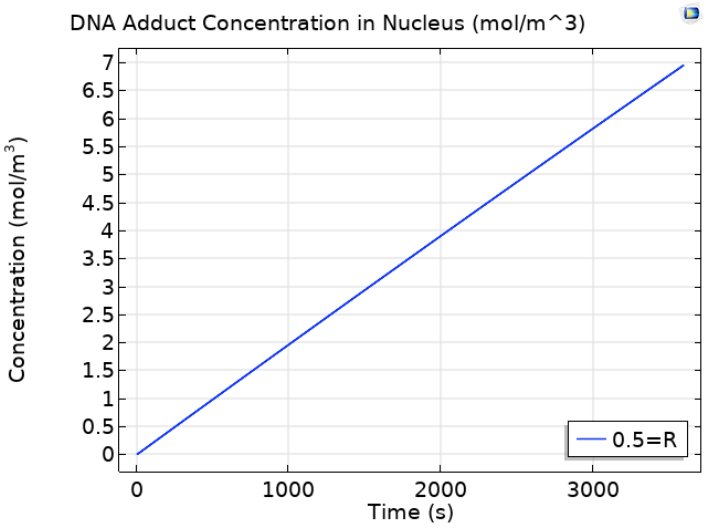

Fig. 8. Concentration of DNA adduct over time at R=0.5

DNA adduct concentration increases throughout the study and will continue to increase until its reactants (Q and AO) run out. The final concentration after 3600 seconds is about 6.95025 mol/m^3. The accuracy of this concentration is discussed in Section 4.2.

4.1 Mesh Convergence

To determine whether the mesh converged, the final DNA adduct concentration inside the nucleus was observed (r = 0.5 um). DNA adducts were chosen because it is the last species in the reaction progression. Therefore, it demonstrates if preceding reactions are converging. More importantly, DNA adducts are the focus of this study. PCB metabolites do not have the potential to be carcinogenic until DNA adducts are formed.

Fig. 9 below shows the mesh convergence. The x-axis indicates solution number, with lower solution numbers corresponding to coarser solutions and higher numbers corresponding to finer solutions. Each "solution number" couples together a maximum element size, maximum element growth rate, and resolution of narrow regions. Due to the nuclear membrane's small size (0.01 um), some custom maximum element sizes were used. Maximum element growth rate and resolution was based on COMSOL presets for mesh sizes. Convergence can be seen at a maximum size of 0.1 um (with a maximum EGR of 1.1 and a resolution of 1, which were based on an "Extremely fine" mesh). A detailed description of parameters for each solution number can be found in Appendix B, Table 13.

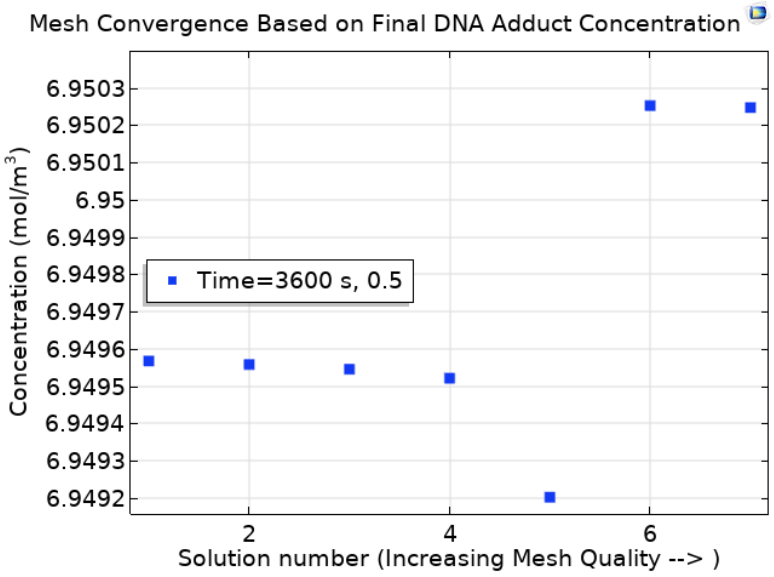

Fig. 9. Mesh convergence at max element size 0.1 um (solution 6)

4.2 Validation

Model validation involved comparing DNA adducts concentration with studies by Zhao et al. and Oakley et al. which observed DNA adduct formation using calf thymus DNA [2, 11]. Formation of DNA adducts after DNA exposure to microsome-generated PCB metabolites (Oakley et al.) or PCB quinones (Zhao et al.) was measured using ^{32}P-post labeling, and calculated via relative adduct labeling (RAL) [2]. RAL is the ratio of count rate for adducted nucleotides to count rate for total nucleotides [13]. Conditions for both studies are shown in Table 5.

Table 5: Comparison of Two Validation Studies

Study	Mammalian cell species	Exposure Temperature(C)	Exposure Time (hrs)	PCB Species (compound)	Species Conc	DNA (ug)	Nucleotides (dGP, ug)
Oakley et al. [11]	Calf thymus	37	3.5	PCB-metabolites (microsome generated)	N/A	150	25
Zhao et al. [2]	Calf thymus	37	48	chlorinated phenyl-1,4-benzoquinone	3 (mg/ml)	400	X

Zhao et al. and Oakley et al. expressed their results with units of number of adducts/ 10^x nucleotides (x= 8 and 9, respectively) [2], [11]. The final DNA adduct results given by our COMSOL model were expressed in mol/m^3. To compare the DNA adduct values, we converted our DNA adduct concentration

to number of adducts/ 10^7 nucleotides based on the following two methods. The final comparison between the two methods and experimental values is shown in Table 6.

4.2.1 Method 1: Stoichiometry

Final adduct concentration from COMSOL was converted to total moles in the nucleus via the nucleus volume, such that:

$$Mol_{Adduct} = C_{Adduct} \times V_{nucleus} = 9.83 \times 10^{-17}(moles) \quad (23)$$

Where: $C_{Adduct} = 6.95025$, $V_{nucleus} = 14.32\ um^3 = 1.432 \times 10^{-17}\ \ m^3$

Assuming 1 mol contains 6.02×10^{23} adducts, based on Avogadro's number, the total number of adducts would be given by:

$$n_{Adduct} = Mol_{Adduct} \times 6.023 \times 10^{23} \quad (24)$$

Based on equation (23), the total number of adducts was calculated to be 5.92×10^7.

We assumed 12 billion nucleotides per cell [18]. Our model would have a total of:

$$\frac{n_{Adduct}}{10^7} = \frac{5.92\times10^7}{1.2\times10^{10}} = 4.929 \times 10^4(adducts/10^7\ nucleotides) \quad (25)$$

4.2.2 Method 2: Conversion Factor

According to [13], the following relation between DNA adduct concentration and DNA adduct molar concentration was obtained.

$$0.3\ pmol\ adduct/mg\ DNA = 1\ adduct/10^7 nucleotides$$

Based on Method 1 above, we can obtain total moles of adduct in the nucleus. Assuming there is 6 pg~6×10^{-9}mg of DNA per cell, we can obtain the total DNA adduct molar concentration for our model [19].

$$Mol_{Adduct} = 9.83 \times 10^{-17}(moles) = 9.83 \times 10^{-5}(picomoles) \quad (26)$$

$$C_{adduct} = \frac{N_{adduct}}{Total\ DNA\ weight(mg)} = \frac{9.83\times10^{-5}}{6\times10^{-9}} = 1.64 \times 10^4 \quad (27)$$

$$C_{final} = C'_{adduct} = C_{adduct}/0.3 = 5.459 \times 10^4(Adduct/10^7 nucleotide) \quad (28)$$

Table.6 Comparison of Literature and Model DNA adduct values.

Calculation Method		Max. Value (Adduct/10^7 Nucleotides)	Min. Value (Adduct/10^7 Nucleotides)
Zhao et al. 2004		4.85 [2]	2.24 [2]
Oakley et al. 1996		1.78 [11]	1.67 [11]
COMSOL Model	Conversion Factor	5.459×10^4	% Difference between 2 Methods
	Stoichiometry	4.929×10^4	10.8%

As seen in Table 6, our model's total number of adducts are about 4 orders of magnitude greater than the experimental values. However, there are multiple possible reasons for this, as discussed in Section 5.

4.3 Sensitivity Analysis

DNA adduct formation rate and quinone formation rate were varied to determine solution sensitivity to these values. DNA adduct concentration was selected for sensitivity analysis because DNA adducts are the final product and focus of this study. Furthermore, Chaudhry et al. did not explain where they obtained their DNA adduct formation rate, so there is a possibility the actual value may vary [20].

DNA adduct concentration was considered sensitive to a parameter if changing the parameter a certain amount produced the same or greater change in DNA adduct concentration.

4.3.1 Sensitivity of k_L and k_{L2}

Quinone formation rate was based on three constants; diol formation rate constant (via epoxide hydrolase), diol transformation rate constant (via dihydrodiol dehydrogenase), and quinone formation rate constant (via peroxidase). Rate of formation of Q was determined (and modeled in COMSOL) by the following equation.

$$c_Q = k_Q \times [(k_{L2} \times [(k_L \times c_{AO})/(1 + k_{L2})]) \,/\, (1 + k_Q)] \tag{29}$$

Therefore, it is likely that the overall quinone formation rate will vary, as it is based on three constants that are also each likely to vary. Furthermore, enzyme kinetics are based on concentration of the enzyme and substrate, temperature, pH, and other factors, so variance is expected.

Table 7 below shows which of the three parameters within the quinone formation rate are most important. Simple numbers were used for all variables to observe trends more easily. Based on the percent difference between the original solution and the solution where single parameters are changed, the diol rate constant

(k_L) is the most important. The diol transformation (k_{L2}) and quinone formation rate constants (k_L) have the same importance, so only one of them needs to be examined in the sensitivity analysis. The diol transformation rate constant (k_{L2}) was chosen because more data is available on its range.

Table.7 Arbitrary Parameter Variation to Determine Inclusion in Sensitivity Analysis

Parameter Changed	cAO (arbitrary)	k_L	k_{L2}	k_Q	Rate of formation Q	Percent Diff
None	10	4	4	4	25.6	0
k_L	10	5	4	4	32	25
k_{L2}	10	4	5	4	26.67	4.17
k_Q	10	4	4	5	26.67	4.17

Table 8 below shows the sensitivity analysis of k_L and k_{L2}, with both parameters altered within the range of values in the SABIO-RK database [21]. Both sensitivity analyses focus on the change in final DNA adduct concentration at 3600 seconds.

Despite changing parameters 4100%, 250%, and 99.6%, the results only changed 89.9%, 35.5%, and 31.9%, respectively. This information is shown in Table 8 as well. Therefore, adduct formation, the main focus of our study, is not sensitive to k_L because the results do not change more than the parameters change.

Table.8 kL and k_{L2} Percent Change and Resulting Percent Change in Final Adduct Concentration

Percent Change in Adduct Concentration @ t=3600 s	Percent Change in k_L	Percent Change in Adduct Concentration @ t=3600 s	Percent Change in k_{L2}
89.86 %	4100 %	6468%	0.20%
35.51 %	250 %	479%	0.014%
-31.88 %	-99.63 %	42.1%	0.0138%

Considering the trend shown in Table 7, if results are not sensitive to k_L, they will not be sensitive to k_{L2}. Table 8 supports this inference. k_{L2} does not significantly impact our results, as even a greater than 1000% change does not change results more than 0.2%. Overall, neither k_L nor k_{L2} impacted our results (adduct concentration) significantly. k_Q will impact the results as k_{L2} did. The formation of quinone overall was not found to be a sensitive parameter.

4.3.2 Sensitivity of DNA Adduct Formation Rate Constant

Assuming the formation of DNA adducts from quinones all follow an analogous reaction mechanism, the DNA adduct formation rate constant of Chaudhry et al., Zhao et al., and Oakley et al. should be similar [9], [2], [11]. Zhao et al. and Oakley et al. quantified the DNA adduct formation rate through ^{32}P-Postlabeling analysis [2],[11]. As shown in Table 9 below, the studies show a 7~9% variation in their final DNA adduct values [211]. This difference in DNA adducts can be attributed to measurement error and possible reaction rate variation. As ^{32}P-Postlabeling analysis is a high sensitivity analysis, with accuracy up to 1 in 10^9 nucleotides, the main source of difference is more likely to be reaction rate variation [23].

The 7-9% variation was applied to DNA adduct formation rate (k_A) for a sensitivity analysis of the final DNA adduct concentration. The resulting changes in final adduct concentration are shown in Table 10.

Table 9: DNA Adduct Concentration Range

Source	Adduct concentration (adduct/10^9 nucleotide)	Range	% Difference
Zhao et al. [2]	22.4	2.1	9
Oakley et al. [11]	178	13	7

Table 10: Sensitivity Analysis Results DNA Adduct Rate Constant(k_A)

% Change in k_A	Final DNA adduct concentration (mol/m^3)	Percent Difference
0 (Original)	6.950	N/A
+7%	7.45	7%
-7%	6.47	7%

A 7% change in DNA adduct formation rate (k_A) results in a 7% change in final DNA adduct concentration. Therefore, because the change in k_A produced the same change in the final DNA adduct concentration, DNA adduct concentration is sensitive to k_A.

5. Conclusion & Design Application

Our initial goal was to model metabolism of a lipophilic compound in a human cell, particularly regarding DNA adduct formation. Unfortunately, it was not possible to validate our model due to the large difference in modeled DNA adducts/10^7 nucleotides versus Zhao et al. and Oakley et al.'s DNA adducts/10^7 nucleotides [2], [11]. A difference of 10^4 is outside our reasonable tolerance for deviation (which would be at most one order of magnitude, not four). However, we believe there to be several

possible sources of error that must be corrected before our model is suitable for proposed design applications.

Time of study and initial concentration of PCB or PCB-metabolite impacts the final number of adducts. For the most accurate validation, the experimental values for time and concentration from Zhao et al. and Oakley et al. should be used in the model (Table 5). The model was run again using the 3.5 hour study time [11]. However, Oakley et al.'s concentration is unknown, so it is not possible to correct for that possible difference [11]. With a longer time, the concentration of DNA adducts increased even more, with final adduct values on the order of 10^5.

For increased accuracy of validation, the concentration of initial PCBs in the model could be manipulated so that the AO and Q concentration is equal to the Zhao et al. Q concentration. However, this is difficult to calculate. While Zhao et al. used a pulse source of Q and a closed system, our "reaction chamber", or the nucleus, has a constant flow of Q and AO coming in to react with the DNA [2]. If we limit the initial PCB concentration in the EC matrix so that the maximum Q and AO formed is equal to the moles of Q used in the Zhao et al. paper, not all of the PCB will diffuse into the cell. So, the actual value of moles of Q and AO reacting with DNA is complicated, and will change depending on the time and concentration.

Although the adduct concentration was not found to be sensitive to rate constants like k_L, k_{L2}, and k_Q, it was found that rate constants vary by factors of 10^6 or more [21]. It is possible that a significantly incorrect rate constant might change our values, considering the wide range. For example, if the largest value for k_L is used, the final adduct concentration is reduced by one order of magnitude. Any k_L that is several orders of magnitude too low may increase DNA adduct concentration by a few orders of magnitude.

Finally, our DNA adduct formation rate was taken from Chaudhry et al. [20]. The source of the value was identified as "unpublished data" [20]. Therefore, it is not possible to determine how this value was obtained, which introduces uncertainty. The adduct concentration is sensitive to the DNA formation rate, as shown in Section 4.3. Thus, if the value for DNA adduct formation is not valid, which we are unable to determine, then a different DNA adduct formation rate may give a final DNA adduct concentration within the expected range.

COMSOL was used to model the diffusion of PCB into a mammalian cell, the subsequent metabolic reactions, and the final accumulation of DNA adducts. Our DNA adduct concentration is 10^4 fold larger than the literature values.

Assuming the model can be corrected to calculate DNA adduct concentrations of the expected magnitude, the model will then be able to predict how much DNA damage will occur after exposure to PCB. It may also be possible to connect this DNA damage to a specified cancer risk. Setting a maximum allowable number of DNA adducts allows one to set a maximum PCB concentration or a maximum time a person can be exposed to. This will allow toxicology study design to be informed by theoretical design and reduce the need for live cell experimentation, potentially saving time and money.

Setting a maximum PCB concentration or exposure time allows one to quantify the minimum amount of PCB to be removed from the physical environment. This constraint could be used in the design of water treatment facilities and technologies, activated carbon beds, and other remediation technologies [24]. If there are any future advancements on techniques to protect the body from PCB or remove PCB and its metabolites from the body, a maximum PCB concentration and exposure time determined by this model could be a necessary design constraint.

The model itself can be a starting block for modeling of metabolic reactions in prokaryotic or eukaryotic cells used in microbial degradation [24]. This would allow prediction of how single celled microorganisms would react to placement in different environments with varying concentrations of PCBs. Time required to remediate a certain PCB concentration and cell tolerance to that concentration could be predicted from the modified model. Cell tolerance to specified PCB concentrations determines how often cells must be replaced, which impacts the cost and feasibility of treatment. The modified PCB-cell model could play an important role in bioremediation process design by allowing one to test different cells and concentrations before working with live cells. Modeling microbial degradation first saves time and money.

By quantifying DNA adducts formed after exposure to different doses of PCB, we can specify maximum allowable PCB exposure in terms of time and concentration. Maximum PCB exposure can be used in remediation technology design and regulations. This COMSOL model may also be adapted to model bioremediation of PCB, which saves time and money. If this model can be corrected to accurately predict DNA adduct formation, it could replace in vitro experimentation, as well as in vivo experimentation on rats and mice. Reducing experimentation on live cells, as mentioned, saves time and money spent on gathering equipment and growing cells. Overall, with improvement, this COMSOL model could inform designs necessary for public and environmental health, as well as saving significant time and money.

References

[1] G. Pinto *et al*, *State of the River Report for the Lower St. Johns River Basin*, WordPress, 2020. Accessed on: Apr. 2, 2021. [Online]. Available: https://sjrr.domains.unf.edu/5-6-polychlorinated-biphenyls-pcbs/

[2] S. Zhao, A. Narang, X. Ding, and G. Eadon, "Characterization and Quantitative Analysis of DNA Adducts Formed from Lower Chlorinated PCB-Derived Quinones," *Chem. Res. Toxicol.,* vol. 17, no. 4, pp. 502-511, 2004. [Online].

[3] M. R. McLean, L. W. Robertson, and R. C. Gupta, "Detection of PCB Adducts by the ^{32}P-postlabeling Technique," *Chem. Res. Toxicol.,* vol. 9, no. 1, pp. 165-171, 1996. [Online].

[4] B. Lauby-Secretan et al., "Carcinogenicity of polychlorinated biphenyls and polybrominated biphenyls", *The Lancet Oncology*, vol. 14, no. 4, 2013, pp. 287-288, doi: 10.1016/S1470-2045(13)70104-9.

[5] L. W. Robertson and G. Ludewig, "Polychlorinated Biphenyl (PCB) carcinogenicity with special emphasis on airborne PCBs," p. 13, 2011.

[6] D. Hu, A. Martinez, and K. C. Hornbuckle, "Discovery of Non-Aroclor PCB (3,3′-Dichlorobiphenyl) in Chicago Air," *Environ. Sci. Technol.*, vol. 42, no. 21, pp. 7873–7877, Nov. 2008, doi: 10.1021/es801823r.

[7] L. A. Rodenburg, J. Guo, S. Du, and G. J. Cavallo, "Evidence for Unique and Ubiquitous Environmental Sources of 3,3′-Dichlorobiphenyl (PCB 11)," *Environ. Sci. Technol.*, vol. 44, no. 8, pp. 2816–2821, Apr. 2010, doi: 10.1021/es901155h.

[8] D. Krewski et al., "Toxicity Testing in the 21st Century: A Vision and a Strategy," *Journal of Toxicology and Environmental Health*, Part B, vol. 13, no. 2–4, pp. 51–138, Jun. 2010. doi: 10.1080/10937404.2010.483176

[9] Q. A. Chaudhry, M. Hanke, and R. Morgenstern. Simulation of Transport of Lipophilic Compounds in Complex Cell Geometry. presented at COMSOL Conference 2009 Milan [Presentation]. Available: https://www.comsol.com/paper/simulation-of-transport-of-lipophilic-compounds-in-complex-cell-geometry-6729

[10] National Research Council (US) Safe Drinking Water Committee, "Biologic Significance of DNA Adducts and Protein Adducts" in *Drinking Water and Health: Volume 9: Selected Issues in Risk Assessment*, 1st ed. Washington (DC), USA: National Academies Press (US), 1989, ch. 1. Available from: https://www.ncbi.nlm.nih.gov/books/NBK218897/

[11] G. G. Oakley, L. W. Robertson, and R. C. Gupta, "Analysis of polychlorinated biphenyl-DNA adducts by ^{32}P-postlabeling," *Carcinogenesis,* vol. 17, no. 1, pp. 109-114, 1996. [Online].

[12] I. G. Sipies and R. G. Schnellmann, "Biotransformation of PCBs: Metabolic Pathways and Mechanisms" in *Environmental Toxin Series 1,* 1st ed. Berlin, Germany: Springer Verlag., 1987, ch. 5, sec. 1-3, pp. 98-108. [Online].

[13] M. V. Reddy and K. Randerath, "^{32}P-Postlabeling Assay for Carcinogen-DNA Adducts: Nuclease P_1-Mediated Enhancement of Its Sensitivity and Applications," *Environmental Health Perspectives*, vol. 76, pp. 41-47, 1987. [Online].

[14] FA Grimm *et al.*, "Metabolism and metabolites of polychlorinated biphenyls," *Crit Rev Toxicol.*, vol. 45, no. 3, pp. 1-75, Mar. 2015. Accessed on April, 13, 2021. doi:10.3109/10408444.2014.999365, [Online].

[15] R. Milo *et al*, *BioNumbers - The Database of Useful Biological Numbers*, Harvard, 2010. Accessed on Mar. 5, 2021. [Online]. Available: https://bionumbers.hms.harvard.edu/search.aspx?trm=CHO&pi=4

[16] H. Cantwell and P. Nurse, "Unravelling nuclear size control," *Curr Genet.*, vol. 65, no. 6, pp. 1281–1285, Dec. 2019. doi: 10.1007/s00294-019-00999-3.

[17] R. Milo *et al*, *BioNumbers - The Database of Useful Biological Numbers*, Harvard, 2010. Accessed on Apr. 2, 2021. [Online]. Available: https://bionumbers.hms.harvard.edu/search.aspx?trm=CHO&pi=4

[18] B. M. Alberts, *et al*, "Introduction," in *Mapping and Sequencing the Human Genome*, 1st edition. United States: The National Academy of Sciences, 1988, ch. 2, sec. 1, p. 16. [Online]. Available: https://www.ncbi.nlm.nih.gov/books/NBK218247/#:~:text=The%20human%20genome%20is%20thus,nucleotide%20on%20the%20other%20strand.

[19] R. Milo *et al*, *BioNumbers - The Database of Useful Biological Numbers*, Harvard, 2010. Accessed on Apr. 18, 2021. [Online]. Available: https://bionumbers.hms.harvard.edu/bionumber.aspx?id=111206

[20] K. Dreij K, Q. A. Chaudhry, B. Jernström , R. Morgenstern, and M. Hanke, "A Method for Efficient Calculation of Diffusion and Reactions of Lipophilic Compounds in Complex Cell Geometry," *PLOS ONE*, vol. 6, no. 8, 2011. [Online].

[21] U. Wittig *et al*, *SABIO-RK - database for biochemical reaction kinetics*, Hits gGmbH, 2012. Accessed on Apr. 2, 2021. [Online]. Available: http://sabio.h-its.org/newSearch/index

[22] U. M. Zanger and M. Schwab, "Cytochrome P450 enzymes in drug metabolism: Regulation of gene expression, enzyme activities, and impact of genetic variation,"

[23] H.H. Schmeiser, M. Stiborova , V. M. Arlt (2013) "^{32}P-Postlabeling Analysis of DNA Adducts." *Methods in Molecular Biology (Methods and Protocols)*, vol 1044. Humana Press, Totowa, NJ. https://doi-org.proxy.library.cornell.edu/10.1007/978-1-62703-529-3_21

[24] R. Jing, S. Fusi, and B. V. Kjellerup, "Remediation of Polychlorinated Biphenyls (PCBs) in Contaminated Soils and Sediment: State of Knowledge and Perspectives," *Frontiers in Environmental Science*, vol. 6, pp. 1-17, Jul. 2018. [Online]. Available: https://www.frontiersin.org/articles/10.3389/fenvs.2018.00079/full

Appendix A

Table 11: Enzyme Details

Model Reaction	Actual Reaction	Enzyme, *Organism*	Rate Constant	Entry ID
PCB → Arene Oxide	H^+ + NADPH + O_2 + Vitamin D3 = H_2O + $NADP^+$ + Calcidiol	Cytochrome p450 27a1'(cholestanetriol 26-monooxygenase), *human*	kcat/Km= 0.48/44= 0.109091 $min^{-1}uM^{-1}$	39031
Arene Oxide → Diol	H_2O+11,12-EET=11,12-DHET	Soluble Epoxide Hydrolase, *human*	kcat/Km = 400,000 $M^{-1}s^{-1}$	68057
PCB → PCB-OH	H^+ + NADPH + O_2 + Vitamin D3 = H_2O + $NADP^+$ + Calcidiol	Cytochrome p450 27a1', *human*	kcat/Km= 0.48/44= 0.109091 $min^{-1}uM^{-1}$	39031
Diol → Cl-Diol	Benzene dihydrodiol + $NADP^+$ = Catechol + NADPH + H^+	trans-1,2-dihydrobenzene-1,2-diol dehydrogenase, *human*	kcat/Km= 19 $min^{-1}mM^{-1}$	1636
Diol → Quinone	H_2O_2 + 3,3',5,5'-Tetramethylbenzidine = H_2O + 4-(4-Imino-3,5-dimethylcyclohexa-2,5-dien-1-ylidene)-2,6-dimethylcyclohexa-2,5-dien-1-imine	Peroxidase, *Human*	kcat/Km= 1235/1.5= 823.33 $min^{-1}mM^{-1}$	64812

Table 12: Model Parameters

Parameter	Constant	Value	Explanation
k_{AO}	Formation rate of Arene Oxides	0.0004545 s^{-1} [21]	0.109091 $min^{-1}uM^{-1}$/ (60 s/min) ×0.25 uM of enzyme[1,2]
k_{PCB-OH}	Formation rate of PCB-OH	0.0004545 s^{-1} [21]	0.109091 $min^{-1}uM^{-1}$/ (60 s/min) ×0.25 uM of enzyme[1,2]
k_{GC}	Formation rate of Glutathione Conjugates	0.3256 s^{-1} [21]	For PAH → PAH-GC
k_L	Formation rate of Diols (L)	0.1 s^{-1} [21]	400000 $s^{-1}M^{-1}$× (1 M/10^6 uM) ×0.25 uM of enzyme[1,2]
k_{L2}	Formation rate of Diol with Cl (L2)	0.000079166 s^{-1} [21]	19 $min^{-1}mM^{-1}$/ (60 s/min) × (1 mM/10^3 uM) × 0.25 uM of enzyme[1,2]
k_Q	Formation rate of Quinones	0.00343 s^{-1} [21]	823.3 $mM^{-1}min^{-1}$/ (60 s/min) × (10^{-3} mM/uM)×0.25 uM enzyme[1,2]
k_A	Formation of DNA Adducts	0.0062 s^{-1} [22]	For PAH→ PAH DNA adducts
D_1	Diffusion coefficient in extracellular matrix	10E-9 m^2/s [11]	For all species in EC matrix (PAH, but not compound specific)
$D_{2,4}$	Diffusion coefficient in membranes	1E-12 m^2/s [11]	For all species in membranes (PAH, but not compound specific)
D_3	Diffusion coefficient in cytoplasm	3.95E-11m^2/s [11]	For all species in cytoplasm (PAH, but not compound specific)
D_5	Diffusion coefficient in nucleus	2.50E-10 m^2/s [11]	For all species in nucleus (PAH, but not compound specific)
k_P	Partitioning coefficient in membranes	4.9×10^{-3} [11]	For all species, same for both membranes
$t_{2,4}$	Membrane Thickness	0.01um [11]	
t_3	Cytoplasm Thickness	5.48 um [15], [16]	
	Cell Diameter	14 um [15]	

	Nucleus Diameter	3 um [16]	
	Extracellular Matrix[4]	50um	
c_{PCB}	PCB Initial Concentration[3]	$306\ \mathrm{mol/m^3}$	Based on Zhao et al. dose [2]

1. Actual reaction in database that corresponds with the rate constant are listed in Table 11

2. 0.25 uM of enzyme was given for a rate constant calculation involving cytochrome P450 [21]. Assumed for all enzymes and reactions.

3. Initial PCB concentration was estimated using Zhao et al's quinone dose of 13.76 $\mathrm{mol/m^3}$ [2]

4. Arbitrarily chosen

Appendix B

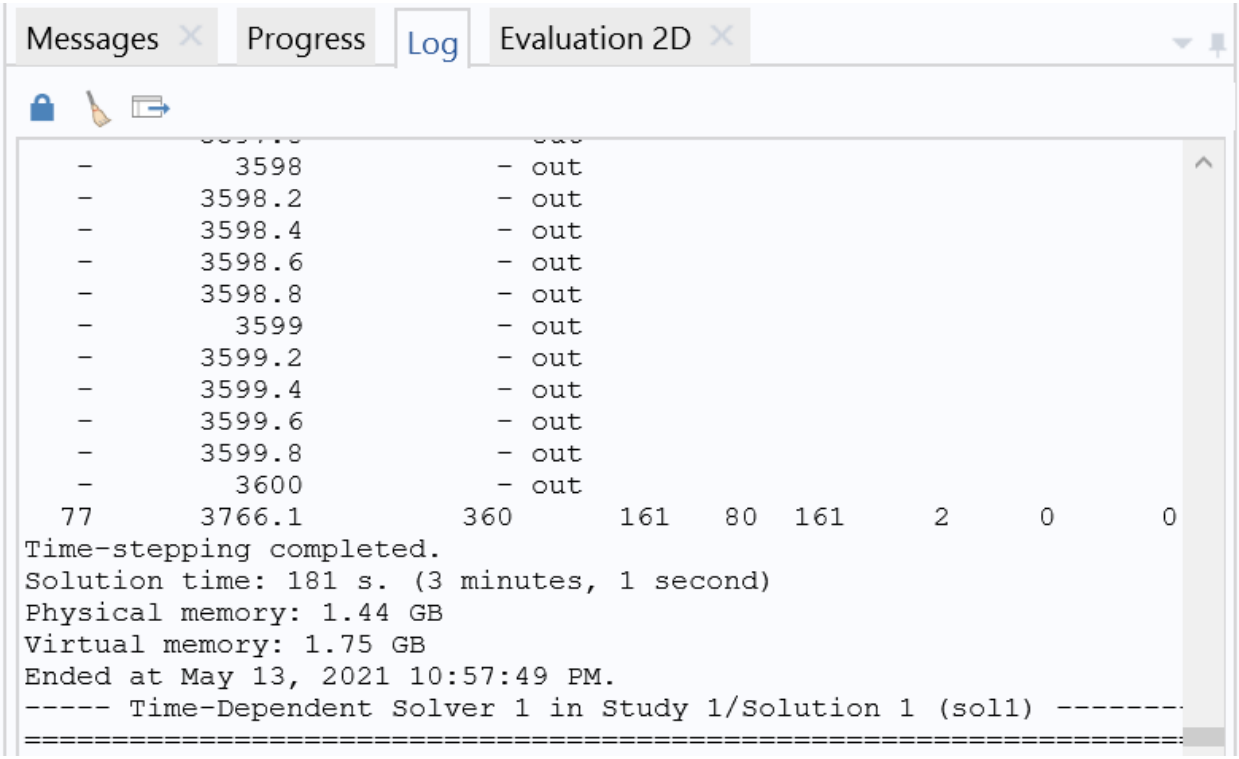

Fig. 10: COMSOL runtime and memory used (experiment run time: 3600 seconds)

A. Computational Methods

The PARDISO direct solver was used, as UMFPACK likely ran out of memory. Fig. 10 above shows the memory used.

Getting mesh convergence required some modification in COMSOL. There was very little change in DNA adduct concentration between different maximum element sizes, so each small deviation appeared as a stark peak or valley. To achieve mesh convergence, maximum element size, maximum element growth rate, and resolution of narrow regions were coupled together using an arbitrary solution number and the parametric sweep's "Specified Combinations" option. Two custom maximum element sizes (combined with the "Extremely Fine" size's EGR and resolution) were added to the parametric sweep; 0.1 and 0.05 um. It was difficult to add enough smaller element sizes without increasing the memory too much. Mesh convergence solution numbers and their corresponding parameters are shown in Table 13 below.

Table 13: Mesh Convergence Solution Number Details

Solution Number	Maximum Element Size (um)	Maximum Element Growth Rate	Resolution
1	3.82	1.3	1
2	3.02	1.3	1
3	2.11	1.25	1
4	1.14	1.2	1
5	0.57	1.1	1
6	0.1	1.1	1
7	0.05	1.1	1

Display of species in all necessary domains required some extra customization due to the nature of the physics. Implementing a partition coefficient required division of PCB, Q, and AO diffusion into 3 separate physics each. For each species, the three physics included the membrane, cytoplasm, and other applicable aqueous domain. To display all domains' concentration for a species on the same plot, an additional parameter was added in each variable table for each domain. Due to the very large concentration difference between the membranes and aqueous domains, the membrane concentration is seldom displayed on the plot with the other domains' concentrations. Including the membrane concentration on a line graph, for example, makes the plot lines jagged where they should be smooth. The concentration of all domains can not be clearly viewed on the same y axis. Therefore, two parameters were created to collect the aqueous domains under one parameter (example: c_Q), and to collect all domains under another parameter (example: CQ). This is shown in Fig. 11 below.

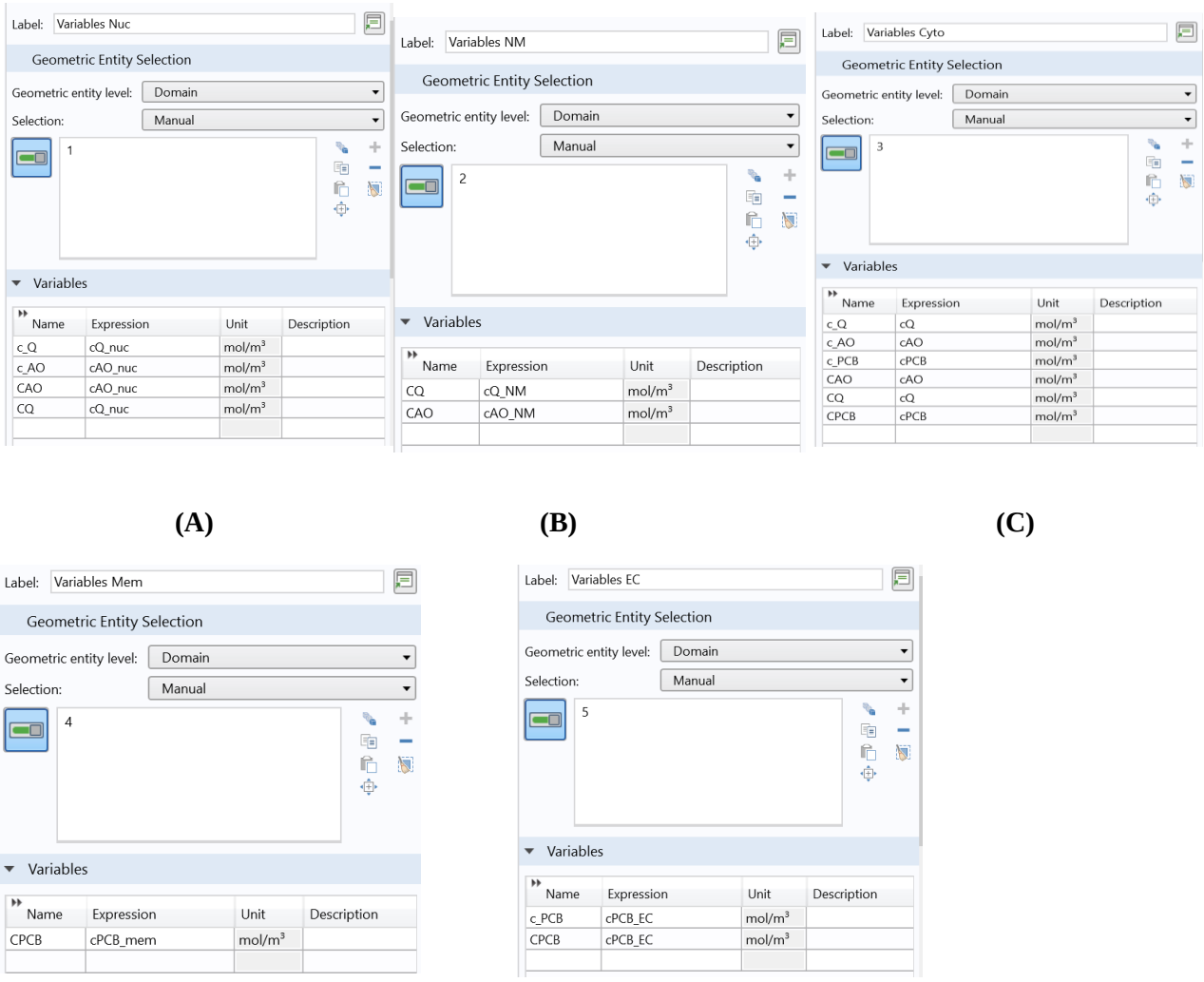

Fig. 11: Variables for each of 5 domains, demonstrating variable relabeling for display ((A) is the extracellular domain, (B) is the cellular membrane, (C) is the cytoplasm, (D) is the nuclear membrane, and (E) is the nucleus)

Partition coefficients were implemented at each lipid-aqueous boundary for each species crossing the boundary, from the perspective of each domain next to the boundary. For PCB, one flux condition was added to the EC physics, two flux conditions were added to the membrane physics (for each side of the membrane), and one flux condition was added to the cytoplasm physics. For AO and Q, one flux condition was added to the cytoplasm physics, two flux conditions were added to the nuclear membrane physics, and one flux condition was added to the nucleus physics. This was done for both species, resulting in a total of 12 fluxes added to address partition coefficients.

Flux was defined in aqueous domain physics as follows in equation 30.

$$Flux = 1000 * (c_{aq.\ reference\ domain} - k_p * c_{adjacent\ membrane\ domain}) \quad (30)$$

Flux was defined in lipid (membrane) domain physics as follows in equation 31.

$$Flux = 1000 * (k_p * c_{membrane\ ref.domain} - c_{aq.\ adjacent\ domain}) \quad (31)$$

The stiff spring constant, which defines the interface sharpness, was chosen to be 1000. k_p is always multiplied by the lipid domain concentration based on the definition of k_p (equations 32 and 33). COMSOL implementation requires that the domain you are currently in and defining the flux for comes first in the equation, and the adjacent domain is subtracted out.

$$k_p = \frac{c_{aqueous}}{c_{lipid}} \quad (32)$$

$$k_p * c_{lipid} = c_{aq} \quad (33)$$

An example of COMSOL implementation is shown below in Fig. 12. Fig. 12A shows definition in the EC for the EC-membrane boundary. Fig. 12B shows definition in the membrane for the EC-membrane boundary. Fig. 16C shows definition in the membrane for the cytoplasm-membrane boundary.

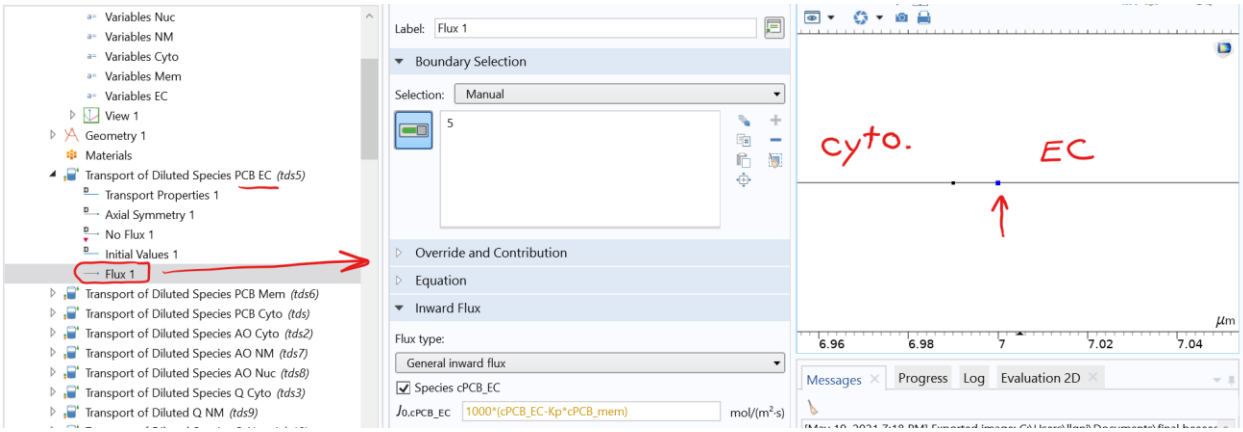

(A)

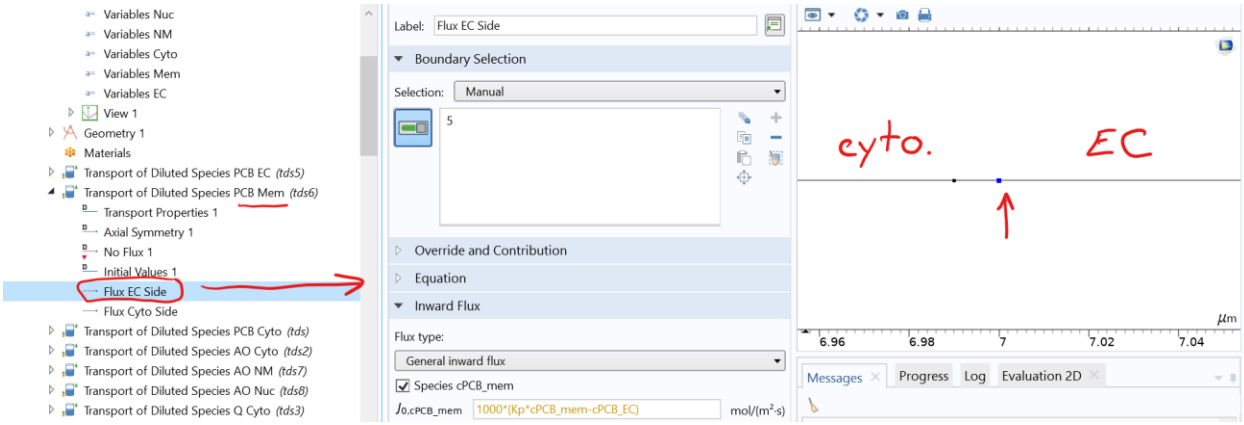

(B)

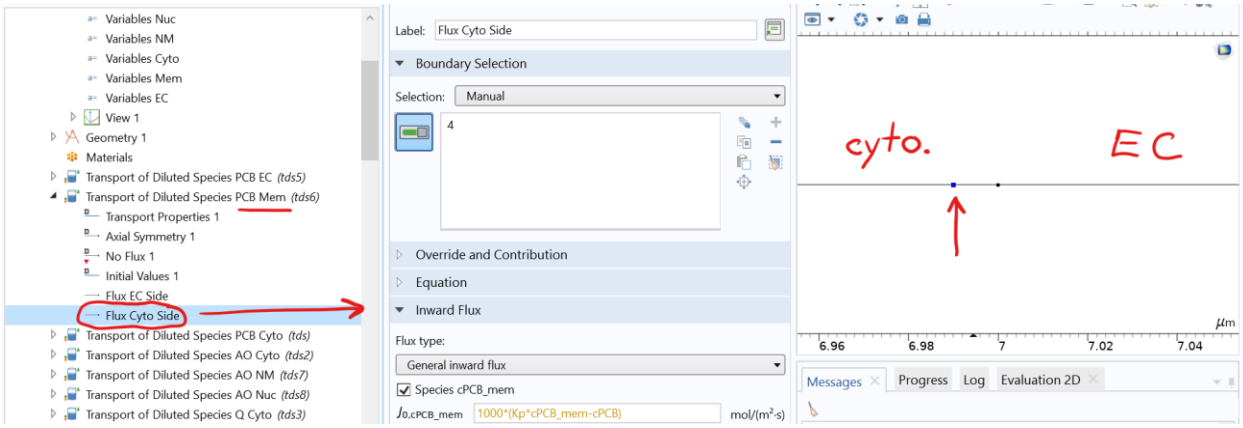

(C)

Fig. 12: Implementation of PCB partition coefficients in COMSOL ((A) is from the extracellular domain at the EC-membrane boundary, (B) is from the cellular membrane at the EC-membrane boundary, (C) is from the cellular membrane at the cytoplasm-membrane boundary)